ACS APPLIED MATERIALS & INTERFACES

Research Article

www.acsami.org

Compositing Polyetherimide with Polyfluorene Wrapped Carbon Nanotubes for Enhanced Interfacial Interaction and Conductivity

Ye Chen, Jing Tao, Song Li, and Niveen M. Khashab*

Controlled Release and Delivery Lab (CRD), Advanced Membranes and Porous Materials Center, King Abdullah University of Science and Technology (KAUST), Thuwal, Makkah 23955-6900, Kingdom of Saudi Arabia

Supporting Information

ABSTRACT: A novel approach to chemically functionalize multiwalled carbon nanotubes (MWCNTs) for making superior polyetherimide (PEI) nanocomposites with polyfluorene polymer is presented. In this approach, MWCNTs are non-covalently functionalized with poly(9,9-dioctyfluorenyl-2,7-diyl) (PFO) through $\pi-\pi$ stacking as confirmed by UV-vis, fluorescence, and Raman spectra. Atomic force microscopy as well as scanning and transmission electron microscopy shows the PFO coated MWCNTs, which provides excellent dispersion of the latter in both solvent and PEI matrix. The strong interaction of PFO with PEI chains, as evidenced from fluorescence spectra, supports the good adhesion of dispersed MWCNTs to PEI leading to stronger interfacial interactions. As a result, the addition of as little as 0.25 wt % of modified MWCNTs to PEI matrix can strongly improve the mechanical properties of the composite (increase of 46% in storage modulus). Increasing the amount of MWCNTs to 2.0 wt % (0.5 wt % PFO loading) affords a great increase of 119% in storage modulus. Furthermore, a sharp decrease of 12 orders of magnitude in volume resistivity of PEI composite is obtained with only 0.5 wt % of PFO modified MWCNT.

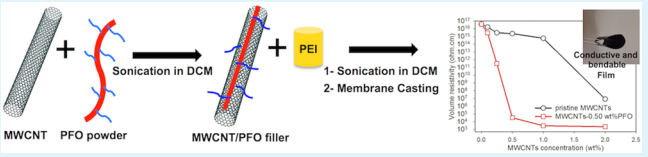

KEYWORDS: *polyetherimide (PEI), poly(9,9-dioctylfluorenyl-2,7-diyl) (PFO), multiwalled carbon nanotubes (MWCNTs), uniform dispersion, interfacial interaction, conductivity*

1. INTRODUCTION

Since their discovery in 1991, carbon nanotubes (CNTs) have drawn lots of interest due to their impressive physical and chemical properties.[1] Their excellent electronic, mechanical, and thermal properties make them great candidates as advanced reinforcing fillers for high-strength, lightweight, and functional polymer nanocomposites.[2−7] Polymer−CNTs composites combine the good processability characteristics of the polymers and the excellent functional properties of CNTs, generating novel light weight low cost material that can be widely applied in different fields such as the electronic industry, aerospace, and the auto industry.

Achieving efficient dispersion of CNTs in polymer matrices remains a challenge, given that they are thermodynamically driven to aggregate by van der Waals forces and $\pi-\pi$ stacking. Moreover, the weak interfacial adhesion of pristine CNTs to polymer matrices dramatically decreases the improvement on polymer properties. Thus, understanding the interfacial interactions between the nanofiller and polymer matrix is important to improve the design and manufacture of polymer nanocomposites. Recent studies have focused on the influence of CNT dispersion on strengthening CNTs−polymer matrix interface interaction, but no generalizations were made in this direction.[8,9] Covalent modifications of CNTs are frequently used in order to improve the weak interfacial adhesion. A notable drawback of covalent functionalization is the disruption of the extended π conjugation in nanotubes, which has a profound effect on their electrical properties.[10−14] Non-covalent functionalization[15−21] has a significant advantage that the chemical groups can be introduced to the CNT surface without disrupting the intrinsic structure and electronic network. Using a polymer or surfactant (including some ionic liquids) to modify CNTs with noncovalent functionalization takes an effective improvement on dispersion of CNTs in solution and polymer matrix.[22−29] Such noncovalent interactions can avoid the destruction of the chemical structure and retain the electric and mechanical properties of CNTs. When molecular surfactants are utilized in the modification process, they can easily form micelles on the surface of nanotubes. However, compared to using polymers, the latter can reduce the entropic penalty of micelle formation[30] and enhance the interaction energy with nanotubes. In fact, as dispersing material, conjugated polymers[31,32] have proved they can enhance the solubility of CNTs in solvent and the resultant composites showed significant improvement in mechanical and electrical properties.[33−35]

Polyetherimide (PEI) is an amorphous polymer with excellent mechanical and thermal performance, such as heat, chemical, fire, and impact resistance. As a thermoplastic, it can be easily reformed after heating and performs successfully in aerospace and auto industries. PEI applications remain limited due to its extremely low conductivity, atmospheric moisture

Received: December 1, 2013
Accepted: January 30, 2014
Published: January 30, 2014

   dx.doi.org/10.1021/am4054805 | ACS Appl. Mater. Interfaces 2014, 6, 9013−9022

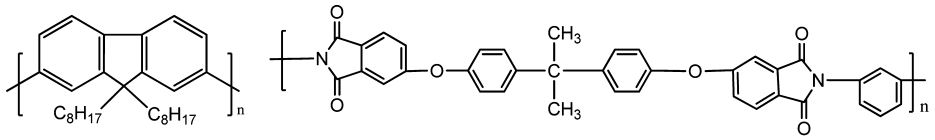

Figure 1. Chemical structure of (a) poly(9,9-dioctylfluorenyl-2,7-diyl) (PFO); (b) polyetherimide (PEI).

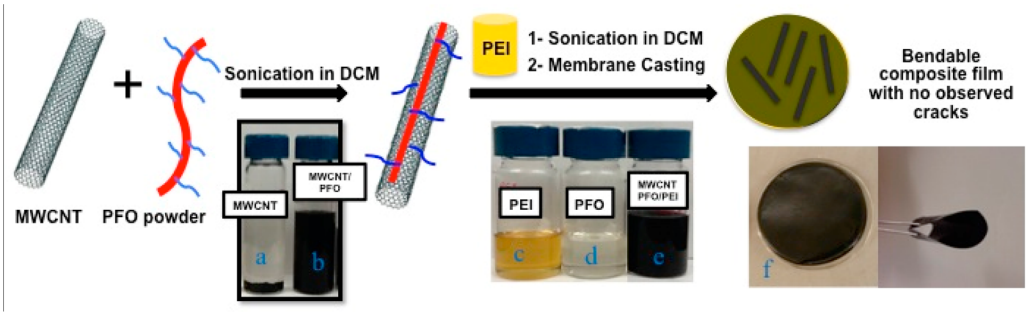

Figure 2. Preparation of PEI−MWCNTs−PFO nanocomposites. (a) Pristine MWCNT precipitate in DCM solvent (0.5 mg/mL MWCNTs in DCM); (b) homogenous solution of PFO−MWCNTs hybrids in DCM (0.5 mg/mL MWCNTs and 0.5 mg/mL PFO in DCM), stable for one month; (c) neat PEI dissolved in DCM (yellow color, 10 wt % PEI concentration); (d) PFO dissolved in DCM (light yellow color, 1.0 wt % PFO concentration); (e) PEI−MWCNTs−PFO solution, the concentration of PFO and MWCNT in PEI solid content is 0.5 wt %; (f) the obtained PEI−MWCNTs−PFO nanocomposite membrane.

absorption, and poor fluidity at high temperature. Different nanofillers including CNTs have been employed to improve PEI properties;[36−42] however, the aggregation, poor load transfer, and interfacial interactions have prevented PEI−CNT nanocomposites from reaching their full potential on an industrially relevant scale.

Current research mainly focuses on improving CNTs dispersion with little to no emphasis on the interfacial adhesion of CNTs to the polymer matrix or the interaction between the solubilizer and the polymer matrix. In this Article, polyfluorene polymer, poly(9,9-dioctylfluorenyl-2,7-diyl) (PFO), is employed to disperse multiwalled carbon nanotubes (MWCNTs) into commercial PEI matrix. PFO has a significant improvement on dispersion of CNTs in organic solvents since it forms a stable hybrid system that wraps the nanotube surface selectively.[43−47] Moreover, both PFO and PEI have aromatic moieties; thus, a good intermiscibility is expected to introduce or mediate the strong interfacial adhesion of MWCNTs into PEI matrix. The resulting PFO−MWCNTs hybrids showed superior interfacial adhesion to the PEI matrix, which drastically enhanced the mechanical and electrical properties of the whole composite. Samples with different PFO−MWCNTs concentrations are prepared, compared, and fully characterized using AFM, SEM, and TEM. Conductivity studies, as well as mechanical and thermal properties of PEI−MWCNTs−PFO composites, are also reported and discussed.

2. EXPERIMENTAL SECTION

2.1. Materials. Polyetherimide (PEI) pellets were supplied by SABIC Innovative Plastics under the trade name of Grade ULTEM 1000P. MWCNTs were purchased from Nanolab Inc. (USA) with diameters of 10−30 nm, lengths of 5−20 μm, and purity of 90% (industrial grade). Poly(9,9-dioctylfluorenyl-2,7-diyl) (PFO) (research grade, average $M_n \sim 15\,834$) was purchased from Sigma-Aldrich and used as received. Figure 1 shows the structures of PEI and PFO. Dichloromethane (DCM), a good solvent for dissolving both PEI and PFO at room temperature, was purchased from Sigma-Aldrich and used without further treatment.

2.2. Preparation of Composite Film. The overall process of preparing PFO−MWCNTs hybrids and PEI−MWCNTs−PFO composite films is presented in Figure 2. PFO fine powder with yellow color was completely dissolved into DCM after stirring for 0.5 h (the obtained homogenous solution is pale yellow). Pristine MWCNTs were first dispersed into DCM under bath-type sonication for 0.5 h and then mixed with PFO solution by sonication for 1 h to form a homogeneous suspension (Figure 2b). PEI chips were dissolved into DCM after stirring for 2 h at 25 °C and then mixed with PFO−MWCNTs solution. The mixture was then stirred for 1 h at room temperature before being treated under bath-type sonication for 1 h. The obtained solutions were casted on a clean glass plate followed by solvent evaporation at room temperature for 24 h. The samples with about 0.3 mm thickness were dried at 80 °C for 24 h to remove any remaining solvent. A series of PEI nanocomposites with different PFO−MWCNTs hybrid concentrations were obtained following the same procedure. The PFO concentration was kept at 0.5 wt % in PEI solid contents, while the concentration of MWCNTs varied from 0.1 to 2.0 wt % in composites. The obtained composite film can be bent without any observed damage (Figure 2f).

2.3. Characterization. *Spectroscopy.* Raman spectroscopy was performed with an ARAMIS UV (HORIBA) Raman Microscope, which is equipped with a 100 mW diode laser with an excitation wavelength of 785 nm. The samples were obtained from thin films casting from their hybrid solution of DCM. The UV-vis spectra were taken in DCM solutions of the samples from 200 to 600 nm using UV-vis spectrophotometer (Varain Cary 5000) at 30 °C. The fluorescence spectra and synchronous fluorescence spectra were obtained from a fluorescence spectrophotometer (Varian Cary Eclipse). Synchronous fluorescence is used to scan the excitation wavelength and emission wavelength at the same time, and then, the fluorescence intensity signal can be obtained. The synchronous fluorescence spectrum has higher selectivity than the common fluorescence spectrum as it can distinguish between similar aromatic polymers. In this study, it was used to investigate the interaction between PFO and PEI.

XRD Study. The X-ray powder diffraction (XRD) patterns were obtained for MWCNTs and PFO hybrids by a Bruker D8 Advance (40 KV, 40 mA) with Cu Kα (λ = 1.5406 Å) irradiation at a scanning rate of 2°/min in the 2θ range of 10−50°.

Microscopy. The dispersion of PFO mixed with MWCNTs in DCM was studied using a transmission electron microscope (TEM, Tecnai T12, FEI Company) operated at accelerated voltage of 120 kV.

A drop of the dilute solution (0.02 mg/mL) of the homogenous mixture on the carbon-coated copper grid was dried in air at room temperature for 2 days. The morphological study of the composite was conducted on a FEI Quanta 600 (USA) scanning electron microscope (SEM). The cryo-fractured surfaces were coated with a thin layer of gold (5 nm). Atomic force microscope (AFM) images were obtained by imaging dried film of dilute suspension on silica using an Agilent 5400 SPM instrument (USA).

Thermal Study. Thermal behavior of the nanocomposites was studied using a differential scanning calorimeter (DSC 204 F1 Phoenix, Netzsch, Germany). The heating rate was 10 °C/min under a nitrogen atmosphere with a flow rate of 20 mL/min. The decomposition behavior was measured by the thermogravimetric analysis (TGA) using Netzsch TG 209 F1 Iris at a temperature range of 30−800 °C under N_2 flow with a heating rate of 10 °C/min.

Mechanical Properties. Dynamic mechanical thermal analysis (DMA) was performed on DMA 242C (Netzsch, Germany) in the tension mode, at a constant frequency of 1 Hz, with the static force at 0.3 N, the dynamic force at 0.2 N, the heating rate of 2 K/min, and in the temperature range of 30 to 250 °C.

Conductivity. Samples for conductivity measurement were prepared in a dimension of 30 × 10 × 0.3 mm^3. A constant voltage of 100 V DC was applied across the specimen using a Keithley model 248 high voltage supply (USA). The current was monitored with a Keithley 6517B (USA) electrometer. The results were obtained by averaging the conductivities from three different specimens for each nanocomposite film.

3. RESULTS AND DISCUSSION

3.1. Characterization of PFO−MWCNTs Dispersion.

PFO is a typical conjugated polymer with the fluorene structure as part of their repeat unit leading to the formation of a stiff backbone. As shown in Figure 2, PFO can be dissolved completely in dichloromethane (DCM) and it can provide a good dispersion for MWCNTs in solvent. The solution of PFO−MWCNTs hybrids was homogenous and stable, and no precipitate of black agglomeration was observed after one month.

Figure 3a shows the UV-vis absorption spectra of PFO dissolved in DCM and PFO−MWCNTs hybrid solutions with varying MWCNT concentrations. It is apparent that neat PFO solution has two peaks at 390 and 436 nm, respectively, which was also observed in other reports.[48−50] The strong absorption at 390 nm belongs to the amorphous structure (α phase) of PFO, indicating PFO exists as a disordered dispersion in DCM. Moreover, the absorption at 390 nm significantly increases by adding MWCNTs into PFO solution, and the peak becomes broader with increasing MWCNT concentrations. The increase of absorption could be caused by the absorbing nature of MWCNTs, and the peak broadening may be related to the interaction of MWCNTs and PFO.[48] The second peak at 436 nm is called β phase, ascribing to the crystal structure of PFO, which is a partial aggregation of PFO chains.[50] The inset in Figure 3a shows an enlarged view of the β phase in UV-vis absorption spectra of PFO−MWCNTs in DCM solutions with varying MWCNT concentrations. It can be observed that β phase peak is suddenly weakened and even disappears with increasing MWCNT concentrations. This transformation indicates that the addition of MWCNTs disturbs the previous structure form of PFO in DCM, and PFO polymer chains become more disordered in DCM with the damage of its partial crystalline phase. The strong interaction of MWCNTs with PFO can be further confirmed by a fluorescence spectrum. As shown in Figure 3b, the fluorescence of PFO is gradually quenched upon addition of MWCNTs. The significant decrease

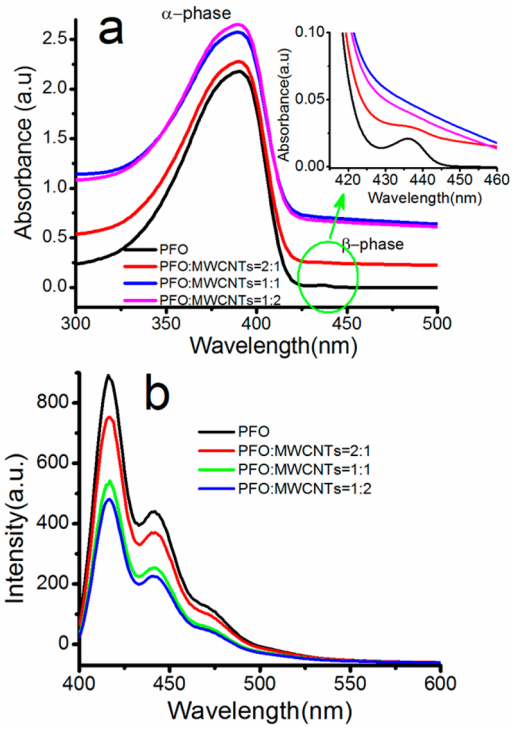

Figure 3. (a) UV-vis spectra of PFO−MWCNTs hybrids in DCM solutions with different PFO−MWCNT weight ratios, keeping the same PFO concentration of 0.2 mg/mL; inset shows the enlarged view of β phase. (b) Fluorescence result of PFO solutions with different MWCNT concentrations.

of PFO fluorescence can be attributed to the transfer of energy from PFO to MWCNTs, supporting a strong interaction between MWCNTs and PFO chains.[51,52] It is also plausible that CNT absorption of the exciting light or absorption of the emitted light is contributing to the decrease in fluorescence; however, fluorescence quenching caused by electron transfer when PFO is mixed with other additives is heavily supported in the literature.[53,54]

TEM images of PFO coated MWCNTs are shown in Figure 4. Compared to pristine MWCNT in Figure 4a, a thick layer of polymer coating is observed on the surface of MWCNT in Figure 4b,c. This can be attributed to the $\pi-\pi$ interactions between conjugated benzene rings of PFO chain and graphitic structure of MWCNT, known for less curvature, as evidenced from UV-vis and fluorescence spectra. This result agrees well with reports of using other aromatic polymers to disperse MWCNTs.[42,54] Moreover, the long aliphatic chains of PFO can improve the overall dispersion of MWCNTs.[21,25]

Atomic force microscopy (AFM) studies further confirm the TEM results. A clear evidence of polymer coating (thicker diameter) on the surface of MWCNT is reported in Figure 5a. The height profile in Figure 5b is consistent with coated MWCNT. In order to avoid AFM tip-induced broadening, the heights are used to analyze the surface of MWCNT rather than width or diameter. From this profile, we can conclude that the diameter of MWCNT is about 40 nm, and the thickness of polymer wrapping on the MWCNT surface is about 35 nm.

Three characteristic bands of pristine MWCNT in the Raman spectrum, 1362, 1581, and 2722 cm^{-1}, can be used to estimate the apparent structural changes that were caused by MWCNT functionalization with PFO (Figure 6a,b; Raman spectrum of pristine PFO is reported in Figure S2, Supporting

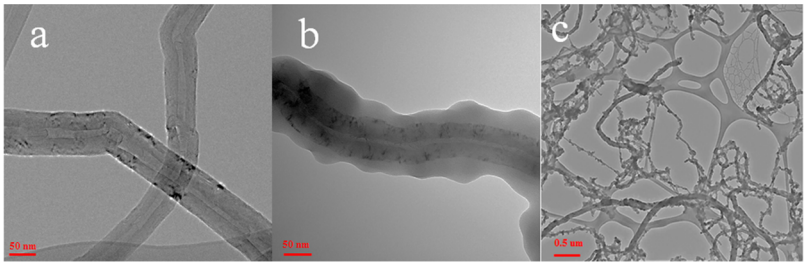

Figure 4. TEM images of (a) pristine MWCNTs; (b) individual MWCNT coated by a layer of PFO; (c) MWCNTs modified with PFO.

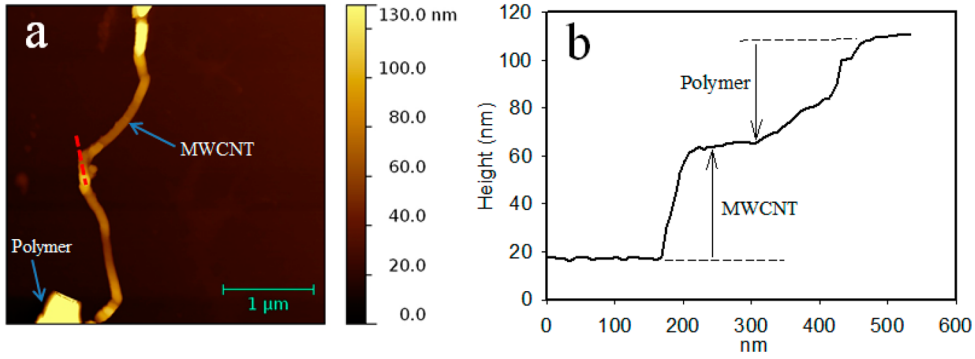

Figure 5. (a) AFM image of individual MWCNT coated by a layer of PFO; (b) height profile along the red dashed line in (a).

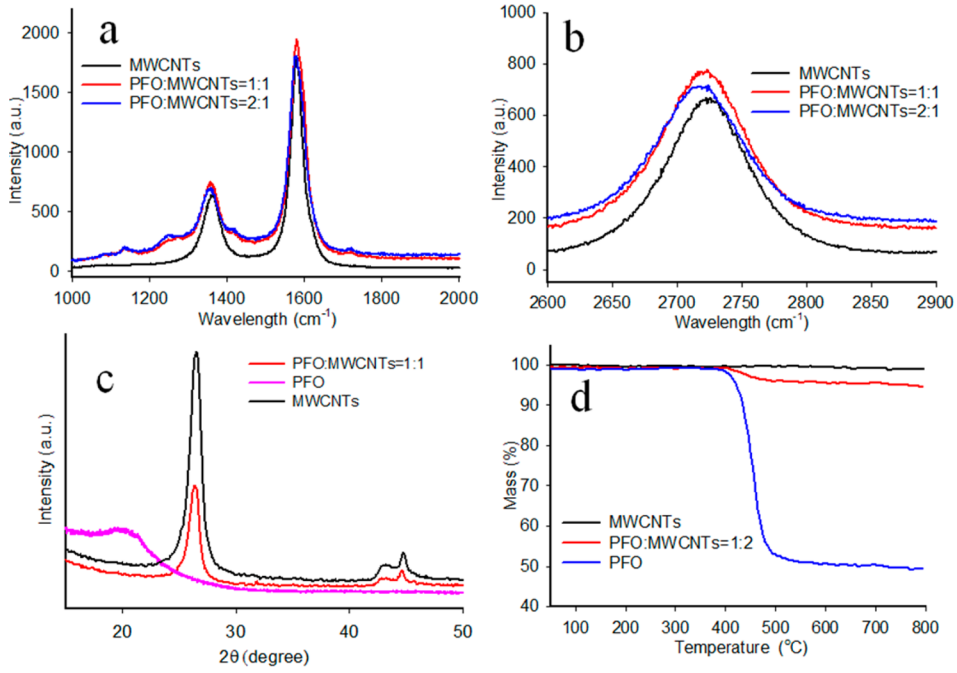

Figure 6. (a, b) Raman spectra of pristine MWCNTs and PFO–MWCNTs hybrids with different PFO–MWCNTs ratios; (c) XRD spectra of pristine MWCNTs, PFO, and their hybrids, respectively; (d) TGA weight loss curves for pristine MWCNTs, PFO, and their hybrids, respectively.

Information). The peak at 1362 cm^{-1} is assigned as a disorder-induced mode (D-band). It has been demonstrated that various disorders, such as confined shapes, edges, disorder between two layers, doping, and atomic defects, give rise to the D-band.[55] The peak at 1581 cm^{-1} is a longitudinal optical (LO) phonon mode, originating from the opposite vibration of carbon atoms in graphite basal layer. This is called G-band using the first letter of "graphite". It is taken as a fingerprint to identify the existence of ordered hexagonal structures in carbon-related materials.[56−58] As shown in Figure 6a, compared to the D-band of pristine MWCNT, the ones for PFO–MWCNTs hybrids exhibited a noticeable Raman shift in the D-band, which became broader probably due to the strong $\pi-\pi$ interaction between PFO and MWCNT. With increasing PFO to hybrid ratio, the D-band shifted to a lower wavenumber, from 1362 cm^{-1} of pristine MWCNT to 1358 cm^{-1} of a complex with a ratio of 2:1 of PFO to MWCNT. The shoulders near D-band at around 1250 and 1420 cm^{-1} and the shoulder near G-band at around 1715 cm^{-1} were also observed in PFO–MWCNTs hybrids. Interestingly, a new peak at 1715 cm^{-1} in the mixture

dx.doi.org/10.1021/am4054805 | ACS Appl. Mater. Interfaces 2014, 6, 9013−9022

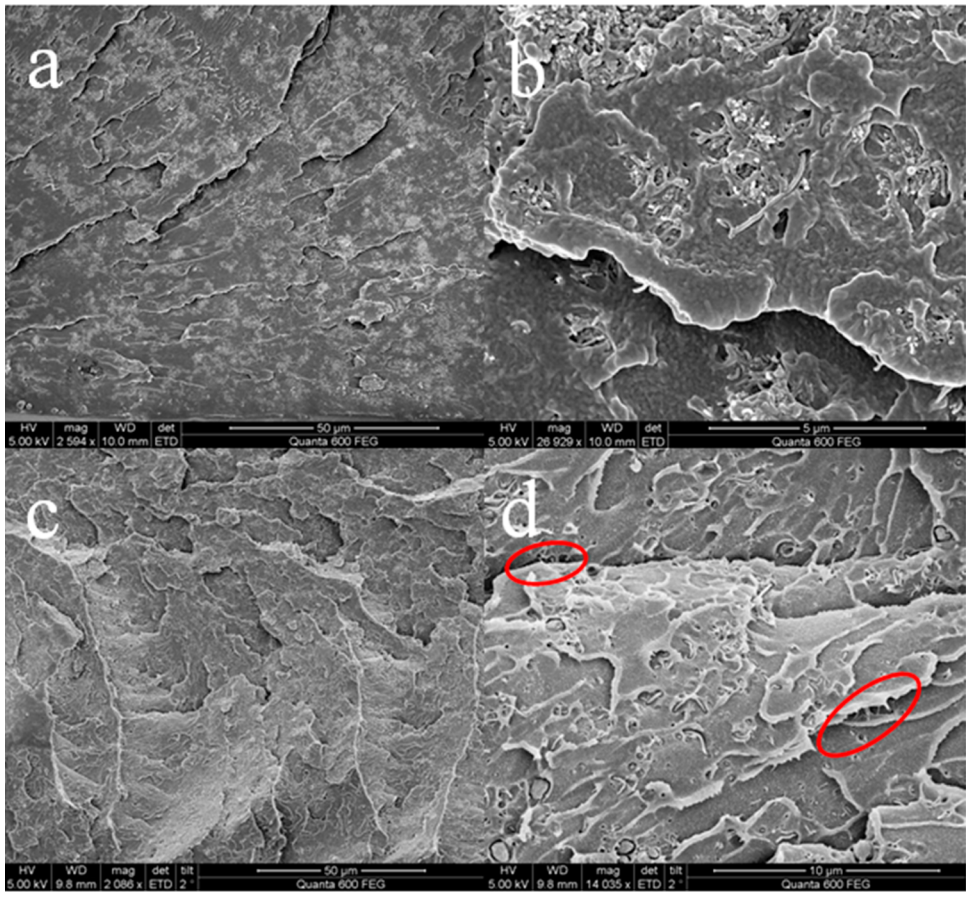

Figure 7. SEM images showing the morphology of the cryo-fractured surface of nanocomposites: (a) PEI nanocomposite with 2.0 wt % pristine MWCNTs; (b) the aggregation of MWCNTs in PEI matrix; (c) PEI nanocomposite with 0.5 wt % PFO and 2.0 wt % MWCNTs; (d) the individual dispersion of MWCNTs in PEI matrix. The red circles show MWCNTs connecting the surface of microcracks.

was observed (not found in neat PFO and pristine MWCNT), which a previous report by Heinz et al. suggested that it may belong to the layer-breathing mode vibration between graphene layers.[59] In our system, PFO chains can form a coplanar arrangement, resulting in an increased π-conjugation.[48] This layer-breathing mode vibration might be observed due to the interaction between the extensively conjugated PFO layer and MWCNT graphitic wall. Another possible reason is that the interaction between PFO chains and MWCNT side-walls influences the vibration of MWCNT layers, which makes the layer-breathing mode vibration visible after modification with PFO. Both scenarios confirm the strong interaction between PFO and MWCNTs. The relative intensity between the D- and the G-bands is known to be a good indicator of the quantity of structural defects. For pristine MWCNTs, the D-band is higher than the G-band, indicating there are many defects in our as-received MWCNTs. The ratio of D-band and G-band of pristine MWCNT is 0.378 and that of PFO−MWCNTs hybrids with mass ratio of 1:1 and 2:1 of PFO to MWCNTs is 0.384 and 0.386, respectively, indicating that non-covalent PFO wrapping had no destructive effects on the surface of CNTs. The higher-order peak that appeared at 2710−2730 cm^{-1} is assigned to a 2D-band, in which the peak position and shape indicates the number of graphene layers. As shown in Figure 6b, compared to pristine MWCNT, the 2D position in MWCNTs wrapped with PFO shifted gradually to lower wavenumber with increasing PFO ratio supporting a strong interaction between MWCNTs and PFO polymer chain.

From XRD patterns of Figure 6c, it can be seen that the diffraction peak at $2\theta = 20.0°$ in neat PFO disappeared in the PFO−MWCNTs hybrid with 1:1 ratio of PFO to MWCNTs, indicating the damage of β phase (crystal structure of PFO) by compositing with MWCNTs. Meanwhile, the characteristic diffraction peaks of pristine MWCNT were maintained after compositing with PFO, indicating the MWCNTs structure is unchanged after functionalization with PFO.

In Figure 6d, the TGA thermograms of pristine MWCNTs, PFO, and PFO−MWCNTs hybrid are presented. PFO has a low decomposition temperature near 390 °C and a 50 wt % weight loss at 800 °C, which means that PFO has poor thermal stability compared with pristine MWCNT which is still stable at high temperature. Compared to neat PFO, the PFO−MWCNTs hybrid has a much better thermal stability. The decomposition temperature of hybrid with 1:2 ratio of PFO to MWCNTs is increased to 415 °C, and the retention rate of the complex at 800 °C still remains above 95 wt %. Therefore, the thermal stability of PFO hybrid is improved as a result of PFO interaction with MWCNTs surface. This further supports the presence of strong interaction between PFO and MWCNTs. Meanwhile, the functionalized MWCNTs can maintain the thermal stability, which is helpful for improving the thermal properties of the composite.

3.2. Characterization of PEI−MWCNTs−PFO Composites. *Morphology of PEI−MWCNTs−PFO Composites.* Scanning electron microscopy (SEM) was employed to study the morphology of the fracture surface for the PEI composite

film containing 2.0 wt % pristine MWCNTs and 2.0 wt % MWCNTs together with 0.5 wt % PFO modification. As shown in Figure 7a, the obvious phase separation is observed in the composite with 2.0 wt % pristine MWCNTs, while the morphology (cross section) of neat PEI is found to be homogenous and smooth (Figure S3, Supporting Information). Aggregation of MWCNTs is dominant in PEI matrix as shown in Figure 7b. However, the addition of PFO strongly improves the dispersion of MWCNTs in PEI matrix (Figure 7c). The morphology of the fracture surface is also homogeneous. In Figure 7d, individual dispersed MWCNT is found in PEI–MWCNTs–PFO composite and throughout the polymer matrix. The individual MWCNT is observed with several micrometers of length in the matrix, indicating no obvious structural damage. The diameter of carbon nanotube coated with polymer is more than 100 nm, which is much bigger than the size of pristine MWCNTs. As shown in TEM and AFM images, the thickness of coated PFO is about 30–40 nm and the size of individual PFO–MWCNTs hybrids is less than the nanotube complex observed in PEI composite. One possible reason is the strong interaction between PEI molecular chain and PFO backbone. Thus, PEI is involved in the coating of MWCNTs surface together with PFO chains and, so, forms a thick polymer complex layer in the nanocomposite. In Figure 7d and S4, Supporting Information, the well-dispersed and coated MWCNTs show good alignment in PEI matrix and act as a bridge across the microcracks, which are the defects of PEI matrix. This linkage of MWCNTs between microcracks provides a release of stress and absorption of energy, which results in a good toughness of PEI nanocomposite.

Interaction between PFO and PEI. As was stated, the two key points for MWCNTs improving polymer composite properties are the MWCNTs being dispersed well in composite matrix and the strong interfacial adhesion of MWCNTs to polymer matrix. SEM and TEM images have directly proved the good dispersion of MWCNTs in PEI matrix, and the strong interaction of MWCNTs with PFO has been disclosed via spectroscopy. In order to understand the interface of modified MWCNTs with PEI, the interaction between PFO and PEI has been investigated by a synchronous fluorescence spectrum. As shown in Figure 8, both characteristic peaks of PEI and PFO clearly shift after mixing. The main characteristic peak of PEI at 448 nm shifts to 445 nm, and the characteristic peak of PFO at 398 nm shifts to 404 nm, respectively. The noticeable Raman shift of PFO and PEI after mixing indicates an existence of strong interaction between PEI and PFO chains, which may result from the π-conjugation structures of PFO backbone interacting with an aromatic amide group of PEI main chain. The existence of this strong interaction between PEI and PFO provides sufficient support for good adhesion of MWCNTs onto PEI matrix. PFO acts as a medium or bridge for strongly linking the MWCNT surface to PEI matrix.

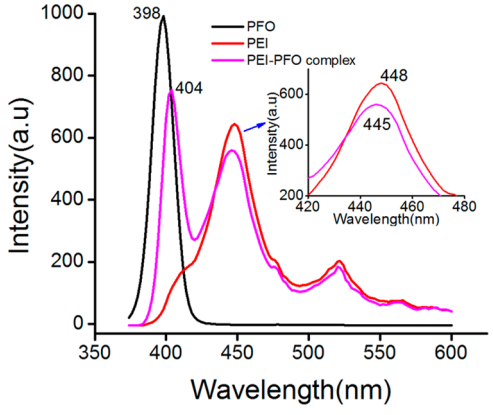

Figure 8. Synchronous fluorescence spectra of PFO, PEI, and PEI–PFO mixture in DCM solvent; inset shows the magnified view of the PEI main characteristic peak. The concentration of PFO in DCM is 0.2 mg/mL, and PEI in DCM is 5 mg/mL.

Thermal Behavior of Composites. As shown in Figure 9a, DSC curves present the distinct glass transition (T_g) of PEI and its nanocomposite membranes. Compared to neat PEI (T_g = 216.9 °C), the T_g is enhanced after incorporating PFO–MWCNTs hybrids, and it can increase further by adding more MWCNTs. There is a 4.6 °C increase in PEI nanocomposite with 0.5 wt % PFO and 2.0 wt % MWCNTs. While in PEI composite with only 2.0 wt % pristine MWCNTs, T_g decreased slightly. The compatibilizer PFO acts as a good interfacial adhesion agent between MWCNTs and PEI matrix, and it plays an important role for dispersing MWCNTs in PEI matrix. The mobility of polymer chains will be reduced due to the constraint effect of MWCNTs. Therefore, the better dispersion of MWCNTs in PEI matrix and higher MWCNT concentrations will bring an increase of T_g, while the aggregation of MWCNTs in polymer matrix could not take any effect on enhancing the stiffness of the polymer; on the contrary, it will reduce its thermal property.

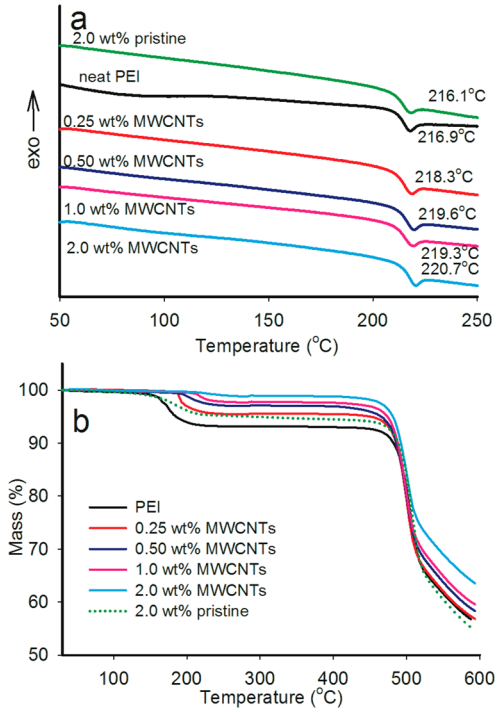

Figure 9. DSC (a) and TGA (b) curves of PEI, PEI composites with 0.5 wt % PFO and different MWCNT concentrations, and PEI composite with only 2.0 wt % pristine MWCNTs.

The thermal stability of neat PEI and its composites was studied by TGA analysis. Two stages are observed in N_2 atmosphere thermal degradation of all samples, as shown in Figure 9b. The first stage between 160 and 210 °C is caused by the presence of labile methyl group present in PEI structure. The weight loss of composites at the same temperature range is

dx.doi.org/10.1021/am4054805 | ACS Appl. Mater. Interfaces 2014, 6, 9013–9022

lowered to 2−6 wt % and even disappears in PEI composite with 0.5 wt % PFO and 2.0 wt % MWCNTs loading, which indicates that the thermal stability is improved by adding MWCNTs modified with PFO. The second stage is the main decomposition of PEI matrix, due to the cleavage of phenylphthalimide bonds.[39] The main decomposition temperature of PEI composite with PFO−MWCNTs hybrid is increased with increasing MWCNT concentrations, while it changes a little with only adding pristine MWCNTs. The data is summarized in Table 1. The thermal stability could be improved by adding carbon nanotubes, because of its excellent thermal stability, and it can slow down the materials' volatilization or decomposition. Meanwhile, the good dispersion of MWCNTs in the polymer matrix restricts the segmental motion of polymer chain, which results in the increase of decomposition temperature.

Table 1. Thermal Properties of PEI and Its Composites

sample	temp. at 10 wt % weight loss (°C)	temp. at 30 wt % weight loss (°C)	weight loss at 400 °C (%)	T_g by DSC (°C)	T_g by DMA (°C)
neat PEI	482	512	7.0	216.9	218.2
0.25 MWCNTs[a]	486	513	4.5	218.3	220.4
0.50 MWCNTs[a]	488	518	3.1	219.6	225.6
1.0 MWCNTs[a]	487	521	2.4	219.3	218.5
2.0 MWCNTs[a]	492	545	1.2	220.7	222.3
2.0 pristine[b]	488	515	5.6	216.1	217.8

[a]PEI composites with 0.5 wt % PFO and different MWCNT concentrations. [b]PEI composite with only pristine MWCNTs.

Dynamic Mechanical Property. DMA curves as a function of temperature for PEI and its nanocomposites are shown in Figure 10. The storage modulus (E') for the PEI composites with PFO−MWCNTs hybrids are higher than that of pure PEI, and the storage modulus increases significantly with increasing MWCNT concentrations (Figure 10a). The results are summarized in Table 2. The storage modulus of composite with 0.25 wt % MWCNTs and 0.5 wt % PFO loading is 2.75 GPa at 50 °C, and it exhibits about 41% increase compared with neat PEI of 1.95 GPa. For the composite containing 2.0 wt % MWCNTs and 0.5 wt % PFO, the storage modulus at 50 °C increased to 4.04 GPa (about 106%). Moreover, the storage modulus of PEI composites with 0.25 wt % MWCNTs and 2.0 wt % MWCNTs shows a 46.0% and 119% increase at 200 °C, respectively. The significant improvement in storage modulus of PEI nanocomposites is ascribed to the combined effect of high performance and fine dispersion of MWCNT filler, as well as the good interfacial adhesion between MWCNTs and PEI matrix. In addition, as shown in Figure 10b, there are two relaxation modes in DMA curves of PEI composites, and the main peak belongs to segmental motion of PEI polymer chain, which showed a similar result with the DSC. The other smaller shoulder is attributed to the motion of PFO chain, which is increased obviously by adding MWCNTs, and it can not be observed in PEI composite with only pristine MWCNTs. Thus, a small amount of PFO can help disperse MWCNTs very well in polymer matrix and increase interfacial interaction and load transfer, which enhances the mechanical properties of the composite.

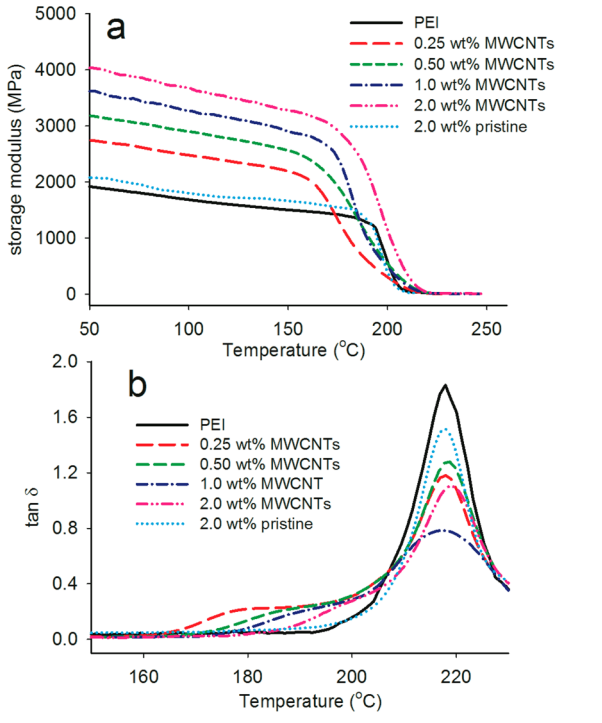

Figure 10. Dynamic mechanical property versus temperature plots of PEI and PEI composites. (a) storage modulus; (b) tan δ versus temperature.

Table 2. Dynamic Mechanical Properties of Neat PEI and Its Composites

sample	storage modulus at 50 °C (GPa)	increase (%)	storage modulus at 150 °C (GPa)	increase (%)
neat PEI	1.95		1.50	
0.25 MWCNTs[a]	2.75	41.0	2.19	46.0
0.50 MWCNTs[a]	3.19	63.6	2.56	70.7
1.0 MWCNTs[a]	3.62	85.6	2.90	93.3
2.0 MWCNTs[a]	4.04	106	3.28	119
2.0 pristine[b]	2.08	6.67	1.66	10.7

[a]PEI composites with 0.5 wt % PFO and different MWCNT concentrations. [b]PEI composite with only pristine MWCNTs.

Electrical Property. The room temperature volume resistivities of PEI and its composites with various concentrations of pristine MWCNTs and modified MWCNTs are shown in Figure 11. The electrical resistivity shows two totally different changing curves with increasing MWCNT concentrations, and it decreases generally with an increase in the content of MWCNTs. For PEI composite with pristine MWCNTs, the volume resistivity decreases smoothly with increasing MWCNTs to 1.0 wt %, and it has a sudden decrease at 2.0 wt % pristine MWCNTs loading. While for PEI composite with MWCNTs modified by using PFO, it shows a better conductivity. The volume resistivity decreases slightly when the MWCNTs content was at 0.1 wt %, from 3.8×10^{16} to 2.8×10^{15} Ω·cm. At this low amount of MWCNTs loading, the MWCNT could disperse separately in PEI matrix; the channels for transporting electrons could not be formed in a large area, which induces a little change of conductivity. With increasing MWCNTs content, the volume resistivity further decreases to 3.1×10^{11} Ω·cm at 0.25 wt % MWCNTs, and then, it sharply decreases to 3.3×10^{4} Ω·cm at 0.50 wt % loading of MWCNTs and 0.50 wt % PFO. The volume

dx.doi.org/10.1021/am4054805 | ACS Appl. Mater. Interfaces 2014, 6, 9013−9022

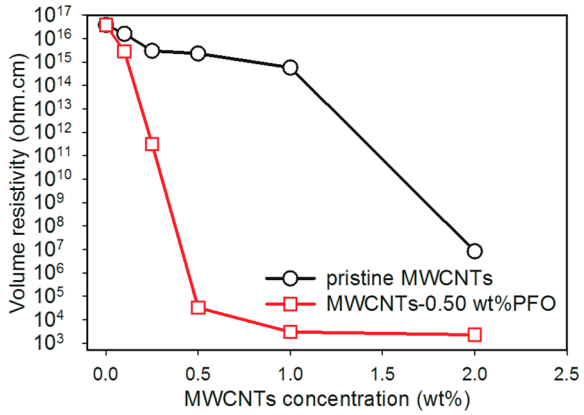

Figure 11. The room temperature volume resistivity of PEI and its composites with 0.5 wt % PFO and different MWCNT concentrations.

resistivity decreases dramatically about 12 orders of magnitude when compared to neat PEI. At this point, the composite can be considered as a semiconductor, but for PEI composite with pristine MWCNTs, it failed to improve PEI conductivity with 0.5 wt % pristine MWCNTs. The resistivity can further decrease with increasing the loading of modified MWCNTs, falling down to 3.0×10^3 Ω·cm at 2.0 wt % loading of MWCNTs and 0.50 wt % PFO. According to the percolation theory,[60] the percolation threshold of the nanocomposites with MWCNTs modified by using PFO is between 0.25 and 0.50 wt %, which means that with the increasing MWCNTs loading, a network forms which provides channels for the electrons transferring throughout the whole matrix. In addition to network formation, the $\pi-\pi$ conjugations of PFO structure and the interaction of PFO with MWCNTs can also help electron transfer between MWCNTs and polymer matrix, which result in a better conductivity with a small amount of MWCNT concentrations. To the best of our knowledge, our obtained resistivity value is one of the lowest for PEI composites (with the same MWCNTs loading) to be reported.

4. CONCLUSION

A simple and fast processing method for high performance PEI nanocomposites based on PFO−MWCNTs hybrids is described. MWCNTs can be separately dispersed in DCM as solvent and homogenously dispersed in PEI matrix by using PFO. The strong interaction between PFO molecular chain and MWCNT and the interaction between PFO and PEI molecular chain provide support to disperse MWCNTs well in PEI matrix and guarantee the good adhesion of MWCNTs with PEI matrix, which are critical for improving load transfer and the overall properties of PEI nanocomposites. The presence of PFO−MWCNTs improved the thermal stability and mechanical property significantly with only 0.25 wt % MWCNTs and 0.5 wt % PFO loading, and these properties were improved further with increasing modified MWCNT concentrations. Meanwhile, the electrical conductivity was enforced by adding PFO−MWCNTs hybrids, and the values increased dramatically by increasing MWCNTs content. This approach provides a straightforward processing method for production of conductive thermoplastics with enhanced interfacial interaction between the filler (PFO−MWCNTs) and the polymer matrix (PEI) that would hopefully lead to better load transfer through the whole composite.

■ ASSOCIATED CONTENT

Ⓢ Supporting Information

AFM images of PFO modified MWCNT, SEM images of neat PEI and PEI with only 0.5 wt % PFO, Raman study of pristine PFO, and microcracks linked by MWCNTs coated with polymer in PEI matrix. This information is available free of charge via the Internet at http://pubs.acs.org/.

■ AUTHOR INFORMATION

Corresponding Author

*Tel:+96628021172. Fax:+96628082410. E-mail: niveen.khashab@kaust.edu.sa.

Notes

The authors declare no competing financial interest.

■ ACKNOWLEDGMENTS

This work was supported by King Abdullah University of Science and Technology (KAUST), Saudi Aramco, SABIC Innovative Plastic Co., and King Abdulaziz City of Science and Technology (KACST). The authors are grateful to Dr. Yang Yang and Dr. Liang Li for their assistance in Raman and XRD analysis.

■ REFERENCES

(1) Iijima, S. Helical Microtubules of Graphitic Carbon. *Nature* **1991**, *354*, 56−58.
(2) Coleman, J. N.; Khan, U.; Blau, W. J.; Gun'ko, Y. K. Small But Strong: A Review of the Mechanical Properties of Carbon Nanotube-Polymer Composites. *Carbon* **2006**, *44*, 1624−1652.
(3) Moniruzzaman, M.; Winey, K. I. Polymer Nanocomposites Containing Carbon Nanotubes. *Macromolecules* **2006**, *39*, 5194−5205.
(4) Diez-Pascual, A. M.; Martinez, G.; Martinez, M. T.; Gomez, M. A. Novel Nanocomposites Reinforced with Hydroxylated Poly(ether ether ketone)-Grafted Carbon Nanotubes. *J. Mater. Chem.* **2010**, *20*, 8247−8256.
(5) Xia, H. S.; Song, M. Preparation and Characterization of Polyurethane-Carbon Nanotube Composites. *Soft Matter* **2005**, *1*, 386−394.
(6) Spitalsky, Z.; Tasis, D.; Papagelis, K.; Galiotis, C. Carbon Nanotube-Polymer Composites: Chemistry, Processing, Mechanical and Electrical Properties. *Prog. Polym. Sci.* **2010**, *35*, 357−401.
(7) Gruner, G. Carbon Nanotube Films for Transparent and Plastic Electronics. *J. Mater. Chem.* **2006**, *16*, 3533−3539.
(8) Bellayer, S.; Gilman, J. W.; Eidelman, N.; Bourbigot, S.; Flambard, X.; Fox, D. M.; De Long, H. C.; Trulove, P. C. Preparation of Homogeneously Dispersed Multiwalled Carbon Nanotube/Polystyrene Nanocomposites via Melt Extrusion Using Trialkyl Imidazolium Compatibilizer. *Adv. Funct. Mater.* **2005**, *15*, 910−916.
(9) Martinez-Rubi, Y.; Ashrafi, B.; Guan, J. W.; Kingston, C.; Johnston, A.; Simard, B.; Mirjalili, V.; Hubert, P.; Deng, L. B.; Young, R. J. Toughening of Epoxy Matrices with Reduced Single-Walled Carbon Nanotubes. *ACS Appl. Mater. Interfaces* **2011**, *3*, 2309−2317.
(10) Price, B. K.; Tour, J. M. Functionalization of Single-Walled Carbon Nanotubes "On Water". *J. Am. Chem. Soc.* **2006**, *128*, 12899−12904.
(11) Hu, H.; Zhao, B.; Hamon, M. A.; Kamaras, K.; Itkis, M. E.; Haddon, R. C. Sidewall Functionalization of Single-Walled Carbon Nanotubes by Addition of Dichlorocarbene. *J. Am. Chem. Soc.* **2003**, *125*, 14893−14900.
(12) Coleman, K. S.; Bailey, S. R.; Fogden, S.; Green, M. L. H. Functionalization of Single-Walled Carbon Nanotubes via the Bingel Reaction. *J. Am. Chem. Soc.* **2003**, *125*, 8722−8723.
(13) Blake, R.; Coleman, J. N.; Byrne, M. T.; McCarthy, J. E.; Perova, T. S.; Blau, W. J.; Fonseca, A.; Nagy, J. B.; Gun'ko, Y. K. Reinforcement of Poly(vinyl chloride) and Polystyrene Using

Chlorinated Polypropylene Grafted Carbon Nanotubes. *J. Mater. Chem.* **2006**, *16*, 4206−4213.
(14) Karousis, N.; Tagmatarchis, N.; Tasis, D. Current Progress on the Chemical Modification of Carbon Nanotubes. *Chem. Rev.* **2010**, *110*, 5366−5397.
(15) Krstic, V.; Duesberg, G. S.; Muster, J.; Burghard, M.; Roth, S. Langmuir-Blodgett Films of Matrix-Diluted Single-Walled Carbon Nanotubes. *Chem. Mater.* **1998**, *10*, 2338−2340.
(16) Star, A.; Stoddart, J. F.; Steuerman, D.; Diehl, M.; Boukai, A.; Wong, E. W.; Yang, X.; Chung, S. W.; Choi, H.; Heath, J. R. Preparation and Properties of Polymer-Wrapped Single-Walled Carbon Nanotubes. *Angew. Chem., Int. Ed.* **2001**, *40*, 1721−1725.
(17) Coleman, J.; Dalton, A.; Curran, S.; Rubio, A.; Davey, A.; Drury, A.; McCarthy, B.; Lahr, B.; Ajayan, P.; Roth, S.; Barklie, R.; Blau, W. Phase Separation of Carbon Nanotubes and Turbostratic Graphite Using a Functional Organic Polymer. *Adv. Mater.* **2000**, *12*, 213−216.
(18) Li, L. Y.; Li, C. Y.; Ni, C. Y. Polymer Crystallization-Driven, Periodic Patterning on Carbon Nanotubes. *J. Am. Chem. Soc.* **2006**, *128*, 1692−1699.
(19) Suri, A.; Chakraborty, A. K.; Coleman, K. S. A Facile, Solvent-Free, Noncovalent, and Nondisruptive Route to Functionalize Single-Wall Carbon Nanotubes Using Tertiary Phosphines. *Chem. Mater.* **2008**, *20*, 1705−1709.
(20) Zhang, L.; Tao, T.; Li, C. Z. Formation of Polymer/Carbon Nanotubes Nano-Hybrid Shish-Kebab via Non-Isothermal Crystallization. *Polymer* **2009**, *50*, 3835−3840.
(21) Vaisman, L.; Wagner, H. D.; Marom, G. The Role of Surfactants in Dispersion of Carbon Nanotubes. *Adv. Colloid Interface Sci.* **2006**, *128*, 37−46.
(22) Zou, J. H.; Liu, L. W.; Chen, H.; Khondaker, S. I.; McCullough, R. D.; Huo, Q.; Zhai, L. Dispersion of Pristine Carbon Nanotubes Using Conjugated Block Copolymers. *Adv. Mater.* **2008**, *20*, 2055−2057.
(23) Guldi, D. M.; Rahman, G. M. A.; Jux, N.; Tagmatarchis, N.; Prato, M. Integrating Single-Wall Carbon Nanotubes into Donor-Acceptor Nanohybrids. *Angew. Chem., Int. Ed.* **2004**, *43*, 5526−5530.
(24) Chen, J.; Hamon, M. A.; Hu, H.; Chen, Y. S.; Rao, A. M.; Eklund, P. C.; Haddon, R. C. Solution Properties of Single-Walled Carbon Nanotubes. *Science* **1998**, *282*, 95−98.
(25) Salavagione, H. J.; Martinez, G.; Marco, C. A Polymer/Solvent Synergetic Effect to Improve the Solubility of Modified Multi-Walled Carbon Nanotubes. *J. Mater. Chem.* **2012**, *22*, 7020−7027.
(26) Fukushima, T.; Kosaka, A.; Ishimura, Y.; Yamamoto, T.; Takigawa, T.; Ishii, N.; Aida, T. Molecular Ordering of Organic Molten Salts Triggered by Single-Walled Carbon Nanotubes. *Science* **2003**, *300*, 2072−2074.
(27) Fukushima, T.; Aida, T. Ionic Liquids for Soft Functional Materials with Carbon Nanotubes. *Chem.−Eur. J.* **2007**, *13*, 5048−5058.
(28) Zhou, J.; Lubineau, G. Improving Electrical Conductivity in Polycarbonate Nanocomposites Using Highly Conductive PEDOT/PSS Coated MWCNTs. *ACS Appl. Mater. Interfaces* **2013**, *5*, 6189−6200.
(29) Chen, Y.; Tao, J.; Deng, L.; Li, L.; Li, J.; Yang, Y.; Khashab, N. M. Polyetherimide/Bucky Gels Nanocomposites with Superior Conductivity and Thermal Stability. *ACS Appl. Mater. Interfaces* **2013**, *5*, 7478−7484.
(30) Britz, D. A.; Khlobystov, A. N. Noncovalent Interactions of Molecules with Single Walled Carbon Nanotubes. *Chem. Soc. Rev.* **2006**, *35*, 637−659.
(31) Rice, N. A.; Soper, K.; Zhou, N. Z.; Merschrod, E.; Zhao, Y. M. Dispersing as-Prepared Single-Walled Carbon Nanotube Powders with Linear Conjugated Polymers. *Chem. Commun.* **2006**, 4937−4939.
(32) Kuila, B. K.; Malik, S.; Batabyal, S. K.; Nandi, A. K. In-Situ Synthesis of Soluble Poly(3-hexylthiophene)/Multiwalled Carbon Nanotube Composite: Morphology, Structure, and Conductivity. *Macromolecules* **2007**, *40*, 278−287.
(33) Coleman, J. N.; Khan, U.; Gun'ko, Y. K. Mechanical Reinforcement of Polymers Using Carbon Nanotubes. *Adv. Mater.* **2006**, *18*, 689−706.
(34) Zou, J. H.; Khondaker, S. I.; Huo, Q.; Zhai, L. A General Strategy to Disperse and Functionalize Carbon Nanotubes Using Conjugated Block Copolymers. *Adv. Funct. Mater.* **2009**, *19*, 479−483.
(35) Kim, K. T.; Jo, W. H. Noncovalent Functionalization of Multiwalled Carbon Nanotubes Using Graft Copolymer with Naphthalene and Its Application as a Reinforcing Filler for Poly(styrene-co-acrylonitrile). *J. Polym. Sci., Part A: Polym. Chem.* **2010**, *48*, 4184−4191.
(36) Lebron-Colon, M.; Meador, M. A.; Gaier, J. R.; Sola, F.; Scheiman, D. A.; McCorkle, L. S. Reinforced Thermoplastic Polyimide with Dispersed Functionalized Single Wall Carbon Nanotubes. *ACS Appl. Mater. Interfaces* **2010**, *2*, 669−676.
(37) Ge, J. J.; Zhang, D.; Li, Q.; Hou, H. Q.; Graham, M. J.; Dai, L. M.; Harris, F. W.; Cheng, S. Z. D. Multiwalled Carbon Nanotubes with Chemically Grafted Polyetherimides. *J. Am. Chem. Soc.* **2005**, *127*, 9984−9985.
(38) Liu, T. X.; Tong, Y. J.; Zhang, W. D. Preparation and Characterization of Carbon Nanotube/Polyetherimide Nanocomposite Films. *Compos. Sci. Technol* **2007**, *67*, 406−412.
(39) Kumar, S.; Li, B.; Caceres, S.; Maguire, R. G.; Zhong, W. H. Dramatic Property Enhancement in Polyetherimide Using Low-Cost Commercially Functionalized Multi-Walled Carbon Nanotubes via a Facile Solution Processing Method. *Nanotechnology* **2009**, *20*, 1−8.
(40) Shao, L.; Bai, Y. P.; Huang, X.; Meng, L. H.; Ma, J. Fabrication and Characterization of Solution Cast MWNTs/PEI Nanocomposites. *J. Appl. Polym. Sci.* **2009**, *113*, 1879−1886.
(41) Jia, X. L.; Zhang, Q.; Zhao, M. Q.; Xu, G. H.; Huang, J. Q.; Qian, W. Z.; Lu, Y. F.; Wei, F. Dramatic Enhancements in Toughness of Polyimide Nanocomposite via Long-CNT-Induced Long-Range Creep. *J. Mater. Chem.* **2012**, *22*, 7050−7056.
(42) Mandal, A.; Nandi, A. K. Noncovalent Functionalization of Multiwalled Carbon Nanotube by a Polythiophene-Based Compatibilizer: Reinforcement and Conductivity Improvement in Poly(vinylidene fluoride) Films. *J. Phys. Chem. C* **2012**, *116*, 9360−9371.
(43) Nish, A.; Hwang, J. Y.; Doig, J.; Nicholas, R. J. Highly Selective Dispersion of Singlewalled Carbon Nanotubes Using Aromatic Polymers. *Nat. Nanotechnol.* **2007**, *2*, 640−646.
(44) Hwang, J. Y.; Nish, A.; Doig, J.; Douven, S.; Chen, C. W.; Chen, L. C.; Nicholas, R. J. Polymer Structure and Solvent Effects on the Selective Dispersion of Single-Walled Carbon Nanotubes. *J. Am. Chem. Soc.* **2008**, *130*, 3543−3553.
(45) Gao, J.; Kwak, M.; Wildeman, J.; Hermann, A.; Loi, M. A. Effectiveness of Sorting Single-Walled Carbon Nanotubes by Diameter Using Polyfluorene Derivatives. *Carbon* **2011**, *49*, 333−338.
(46) Gao, J.; Loi, M. A.; de Carvalho, E. J. F.; dos Santos, M. C. Selective Wrapping and Supramolecular Structures of Polyfluorene-Carbon Nanotube Hybrids. *ACS Nano* **2011**, *5*, 3993−3999.
(47) Gao, J.; Loi, M. A. Photophysics of Polymer-Wrapped Single-Walled Carbon Nanotubes. *Eur. Phys. J. B* **2010**, *75*, 121−126.
(48) Bansal, M.; Srivastava, R.; Lal, C.; Kamalasanan, M. N.; Tanwar, L. S. Change in Conformation of Polymer PFO on Addition of Multiwall Carbon Nanotubes. *Nanoscale* **2010**, *2*, 1171−1177.
(49) Alam, M. M.; Jenekhe, S. A. Binary Blends of Polymer Semiconductors: Nanocrystalline Morphology Retards Energy Transfer and Facilitates Efficient White Electroluminescence. *Macromol. Rapid Commun.* **2006**, *27*, 2053−2059.
(50) Huang, L.; Huang, X. A.; Sun, G. N.; Gu, C.; Lu, D.; Ma, Y. G. Study of Beta Phase and Chains Aggregation Degrees in Poly(9,9-dioctylfluorene) (PFO) Solution. *J. Phys. Chem. C* **2012**, *116*, 7993−7999.
(51) Chen, J.; Liu, H. Y.; Weimer, W. A.; Halls, M. D.; Waldeck, D. H.; Walker, G. C. Noncovalent Engineering of Carbon Nanotube Surfaces by Rigid, Functional Conjugated Polymers. *J. Am. Chem. Soc.* **2002**, *124*, 9034−9035.
(52) Nish, A.; Hwang, J. Y.; Doig, J.; Nicholas, R. J. Direct Spectroscopic Evidence of Energy Transfer from Photo-Excited

Semiconducting Polymers to Single-Walled Carbon Nanotubes. *Nanotechnology* **2008**, *19*, 1−8.
(53) Feng, X. L.; Lv, F. T.; Liu, L. B.; Tang, H. W.; Xing, C. F.; Yang, Q. O.; Wang, S. Conjugated Polymer Nanoparticles for Drug Delivery and Imaging. *ACS Appl. Mater. Interfaces* **2010**, *2*, 2429−2435.
(54) Baykal, B.; Ibrahimova, V.; Er, G.; Bengu, E.; Tuncel, D. Dispersion of Multi-Walled Carbon Nanotubes in an Aqueous Medium by Water-Dispersible Conjugated Polymer Nanoparticles. *Chem. Commun.* **2010**, *46*, 6762−6764.
(55) Wang, Y.; Alsmeyer, D. C.; Mccreery, R. L. Raman-Spectroscopy of Carbon Materials - Structural Basis of Observed Spectra. *Chem. Mater.* **1990**, *2*, 557−563.
(56) Kawashima, Y.; Katagiri, G. Fundamentals, Overtones, and Combinations in the Raman-Spectrum of Graphite. *Phys. Rev. B* **1995**, *52*, 10053−10059.
(57) Dresselhaus, M. S.; Dresselhaus, G.; Saito, R.; Jorio, A. Raman Spectroscopy of Carbon Nanotubes. *Phys. Rep.* **2005**, *409*, 47−99.
(58) Malard, L. M.; Pimenta, M. A.; Dresselhaus, G.; Dresselhaus, M. S. Raman Spectroscopy in Graphene. *Phys. Rep.* **2009**, *473*, 51−87.
(59) Lui, C. H.; Malard, L. M.; Kim, S.; Lantz, G.; Laverge, F. E.; Saito, R.; Heinz, T. F. Observation of Layer-Breathing Mode Vibrations in Few-Layer Graphene through Combination Raman Scattering. *Nano Lett.* **2012**, *12*, 5539−5544.
(60) Ounaies, Z.; Park, C.; Wise, K. E.; Siochi, E. J.; Harrison, J. S. Electrical Properties of Single Wall Carbon Nanotube Reinforced Polyimide Composites. *Compos. Sci. Technol.* **2003**, *63*, 1637−1646.